Jungyong Wang
Faculty of Engineering and Applied Science,
Memorial University of Newfoundland,
St. John's, NL, A1B 3X5, Canada
e-mail: Jungyong.Wang@nrc-cnrc.gc.ca

Ayhan Akinturk

Stephen J. Jones

Institute for Ocean Technology,
National Research Council Canada,
St. John's, NL, A1B 3T5, Canada

Neil Bose
Faculty of Engineering and Applied Science,
Memorial University of Newfoundland,
St. John's, NL, A1B 3X5, Canada

Moon-Chan Kim

Ho-Hwan Chun

Department of Naval Architecture & Ocean Engineering,
Pusan National University,
30 Changjeon-dong, Kumjeng-ku,
Busan, Korea, 609-735

Ice Loads Acting on a Model Podded Propeller Blade (OMAE2005-67416)

With the increase in popularity of podded propulsors and arctic navigation, understanding the interaction between a podded propulsor and ice has become more important. Propeller-ice interaction itself is a complicated process with a high level of uncertainty resulting from the uncertainties associated with the properties of the ice and with the propeller-ice interaction conditions. Model tests provide relatively well-controlled ice properties and interaction conditions to reduce the uncertainties. In order to improve the understanding of this interaction and to develop numerical models of it, a model podded propulsor was used in "Puller" mode, and ice loads were measured on its instrumented blade and propeller shaft. The results of the experiments conducted to simulate the interactions (milling) of the instrumented blade with ice in different operating conditions are reported in this paper. Loads measured during the milling consist of ice milling loads, "inseparable" hydrodynamic loads, and "separable" hydrodynamic loads. The sample results presented here include ice milling and inseparable hydrodynamic loads for various advance coefficients and depths of cut (amount of blade penetration into ice). Some results are compared with existing ice load models. [DOI: 10.1115/1.2426993]

Keywords: ice class, propeller, propeller-ice interaction, model test, ice tank

Introduction

The problem of propeller-ice interaction has been investigated for many years. Among the approaches to understand the interaction are full-scale trials, model tests, and numerical simulations. Full-scale trials are expensive. Precise information about the ice properties in full-scale trials are usually insufficient, hence, the level of uncertainty is increased in the measured data. On the other hand, conducting model tests is useful to obtain more accurate information regarding ice properties and interaction conditions, and measured data.

The interaction itself is a complex process owing to the high strain rates (because of high propeller blade tip velocities), complexity of the flow around the circumference of a propeller, and the randomness in the shape and the way of an ice piece interacting with a propeller. The objective of this study is to improve the understanding of this complex phenomenon, through model tests, and to develop numerical models to predict the loads acting on a propeller blade in milling conditions.

Full-scale measurements for propeller-ice interaction have been presented by several researchers [1–5]. In [6–10], models of the interaction from the experimental and theoretical points of views are given as part of Joint Research Project Arrangement 6 (JRPA #6). References [11–14] report on the experimental findings and new interaction models. Searle et al. [13] tested both an R-Class icebreaker propeller and a highly skewed propeller. Moores et al. [14,15] tested a highly skewed propeller and measured the forces and moments due to ice acting on a single blade. The tests conducted by Moores and his colleagues [14,15] were the first successful tests to accurately measure blade loads during ice milling. They used a blade dynamometer that was designed to accurately distinguish blade load components: three orthogonal force and moment components. Other numerical and empirical studies were carried out to understand the ice load acting on a propeller blade [10–12,16]. Noncontact hydrodynamic forces resulting from propeller blockage are reported in [17–21].

This paper presents results from experiments conducted at the IOT's ice tank with a model podded propulsor. The experiments consisted of tests in open water and in ice covered water. In the ice covered water tests, the propeller milled the ice from underneath an ice sheet at varying depths of cut, propeller rotational speeds, and advance velocities. The total load on a blade during these tests in ice can be expressed as given in Eq. (1). It is assumed to have three components: "*separable*" and "*inseparable*" hydrodynamic loads and ice contact (milling and/or impact) loads. *Ice-related* loads are obtained by subtracting the results of open water tests, which are "*separable*" hydrodynamic loads, from the tests in ice covered water. The "*inseparable*" hydrodynamic loads are caused by the blockage effects, proximity effects, and cavitation.

$$\text{Total loads in ice} = \text{ice milling loads} + \text{"}\textit{separable}\text{" hydrodynamic loads} + \text{"}\textit{inseparable}\text{" hydrodynamic loads}$$

Contributed by the Ocean Offshore and Arctic Engineering Division of ASME for publication in the JOURNAL OF OFFSHORE MECHANICS AND ARCTIC ENGINEERING. Manuscript received January 3, 2006; final manuscript received September 25, 2006. Assoc. Editor: Ge (George) Wang. Paper presented at the 24th International Conference on Offshore Mechanics and Arctic Engineering (OMAE2005), June 12–17, 2005, Halkidiki, Greece.

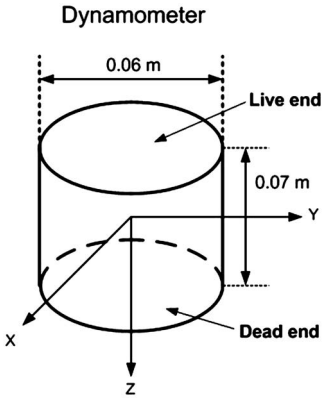

Fig. 1 Dimensions of the AMTI dynamometers

$$\text{"}ice\text{-}related\text{"}\ \text{loads} = \text{ice milling loads} + \text{"}inseparable\text{"}\ \text{hydrodynamic loads} \quad (1)$$

Experimental Tests

Measurements. The model podded propulsor had three six-component dynamometers installed to measure blade loads and shaft-bearing loads. The blade dynamometer was attached to one of the blades inside the hub, and aft and forward dynamometers were mounted on the shaft bearings. These three dynamometers were identical, as shown in Fig. 1. They were manufactured by Advanced Mechanical Technology Inc. (AMTI) and were capable of measuring forces/moments in six degrees of freedom. They could measure forces up to 2224 N in x and y directions, 4448 N in the z direction, and moments up to 56.5 Nm about all three axes. The AMTI load cell model number for all three dynamometers was MC2.5-6-1000. The axes for the blade dynamometer are shown in Fig. 2.

Additionally, strain gauges were mounted on the propeller drive shaft for shaft torque measurements. Shaft thrust was calculated using the information obtained from the aft and forward dynamometers. Blade angular position was measured by a rotary position transducer, Waters WPM Model 18-09. The three dynamometers, shaft torque, and blade angular position were sampled at a rate of 5000 Hz, because the propeller rotational speed was high and many data points were needed during propeller-ice interaction.

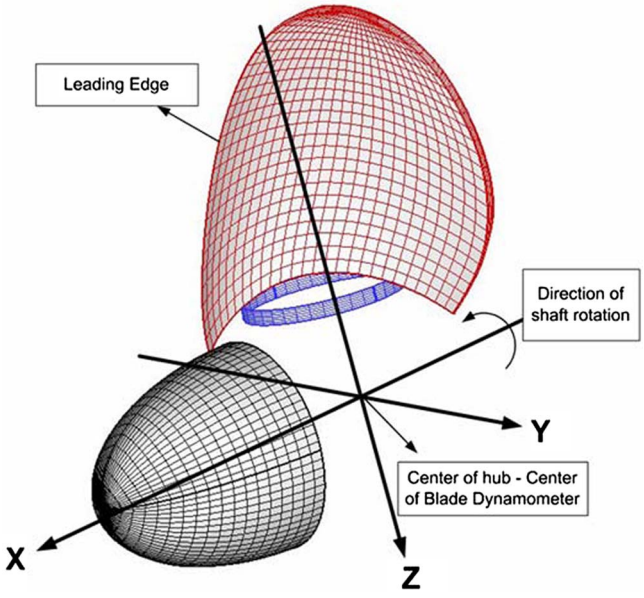

Fig. 2 Axes for blade dynamometer

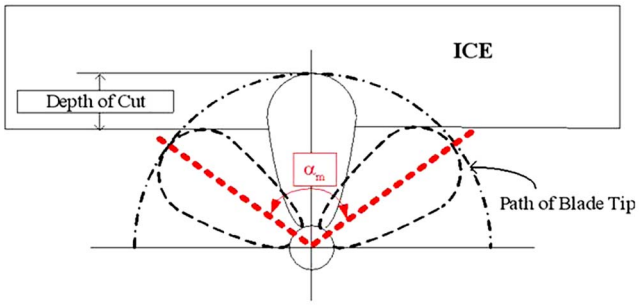

Fig. 3 Depth of cut and milling angle

Propeller rotational speed and carriage speed were sampled at a rate of 50 Hz. Depths of cut were measured manually after each run to ensure accurate values. Given a depth of cut, the milling angle (α_m) is defined using the blade angular position as shown in Fig. 3. During the course of the experiments, the thickness, flexural, compressive, and shear strength values of the ice sheets were sampled at approximately 2 hour intervals in order to record the variations in the ice properties. Akinturk et al. [22] and Wang et al. [23,24] show some results obtained with the present experimental model, including global loads acting on the whole pod system, effects of azimuthing angle, and open water results.

Model Podded Propulsor/Ice Tank. A sketch of the model podded propulsor in "puller" mode is shown in Fig. 4. The model propeller has a similar design to the propellers for the Canadian Coast Guard Gulf/River Class Medium Icebreaker Ships (R Class propeller). The propeller has a diameter of 0.3 m and four blades. Mean-pitch/diameter ratio (P/D) is 0.76 and expanded blade area ratio (EAR) is 0.669. The blade design is based on the Stone Marine Meridian series [25], but the blades are thickened for operation in ice. The diameter of the hub at the propeller is 0.11 m. The propeller shaft was driven by a 3.3 kW electric drive motor.

The tests were conducted in the Ice Tank at the Institute for Ocean Technology, National Research Council of Canada [26]. The usable area of the tank for ice testing is 76 m long, 12 m wide, and 3 m deep. In addition, a 15 m long setup area is separated from the ice sheet by a thermal door to allow equipment preparation while a test sheet is prepared (Fig. 5). The range of the carriage speed is from 0.0002 to 4.0 m/s. The carriage is designed with a central testing area where a test frame, mounted to the carriage frame, allows the experimental setup to move transversely across the entire width of the tank. In order to maximize the use of an ice sheet, each ice sheet was precut into three longitudinal parts; they were called the North, Center, and South Channels. For the tests in ice covered water, the Centre Channel was used first, then the South and North Channels were to follow with stiffeners to keep them in place.

Model Ice/Ice Conditions. Model EG/AD/S ice was used in these experiments. EG/AD/S ice is specifically designed to provide the scaled flexural strengths of columnar sea ice [27,28]. It is a diluted aqueous solution of ethylene glycol (EG), aliphatic detergent (AD), and sugar (S). First, the ice sheet is grown by cooling the tank room to approximately −20°C and then "seeding" the tank by spraying warm water into the cold air in a thin mist, allowing it to form ice crystals before it contacts the surface of the tank. The ice is then allowed to grow at approximately −20°C until it has reached the desired thickness. The temperature of the room is then raised to above freezing and the ice is allowed to

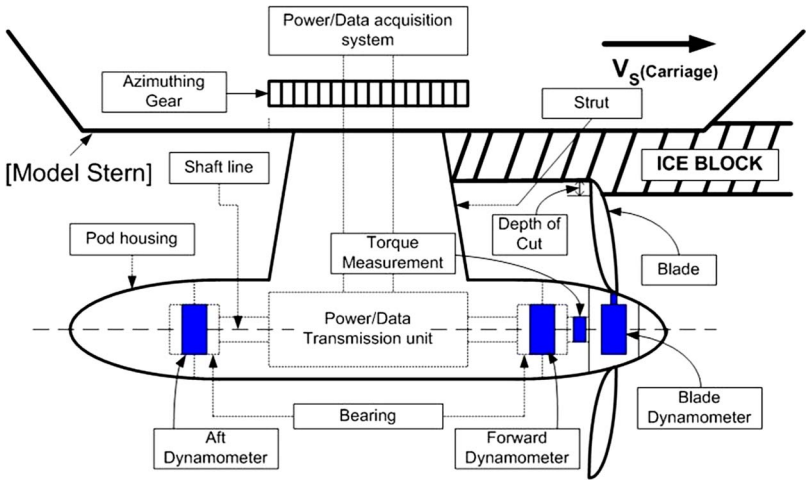

Fig. 4 Apparatus of the "puller mode" podded propulsor

warm up and soften, a process called tempering, until the target ice strength is reached. In order to match the correct scaled density, micro-bubbles are used in the formation of an ice sheet. This process introduces heterogeneous ice properties across the sheet. Since for this study an ice sheet with uniform properties was more important, micro-bubbles for the correct density scaling were not applied to the ice sheets.

The tests in ice covered water were conducted in pre-sawn ice for two different depths of cut: 15 and 35 mm. For this study, the target thickness and flexural strength were 60 mm and 80 kPa, respectively. Figures 6 and 7 show the properties of the model ice during the tests. The vertical axis shows the magnitudes of the compressive, flexural, and shear strengths, and the horizontal axis shows the time elapsed since the first sample is taken (present tests had been carried out for several hours). The mean compressive strength values for 35 and 15 mm depths of cut were 210 and 120 kPa, respectively. Table 1 shows the test matrix. Several runs were repeated at the same condition for a repeatability study.

Data Analysis

Figure 8 shows the time series data from one of the tests. The upper three graphs show F_X, F_Y, and F_Z and the middle three graphs show M_X, M_Y, and M_Z, respectively, for the key blade, to which the blade dynamometer was attached. The bottom two graphs show the blade angular position and carriage speed respectively. These graphs except for the carriage speed are plotted over a 1 s interval, the 65th to 66th seconds. In the time series records for the forces and moment, five peaks can be seen because the propeller rotational speed was 5 rps. The carriage speed for the duration of the 65th and 66th seconds was 0.5 m/s.

In order to obtain "*ice-related*" loads, the milling angle (α_m) that corresponded to the depths of cut was considered (Fig. 3 and Table 2). It is assumed that the ice thickness and the depth of cut were the same as the target values during these tests.

Since the blade angular position was recorded simultaneously with the other measurements, if the milling angle is known, then the corresponding segments for all force and moment components can be identified. In Fig. 9, the "*ice-related*" loads, for which the "*separable*" hydrodynamic loads were removed, are shown by open triangles. For the results presented in this paper, the propeller rotated counter-clockwise, and the blade angular position was measured up to positive and negative 180 deg. In Fig. 9, the blade angular position for the milling period is from 36 to −69 deg for the 35 mm depth of cut. The milling period is the period when the blade is in contact with the ice.

Due to its mechanical limitations, from approximately −160 to −180 deg, the blade angular position sensor had a dead zone and did not record the position. This dead zone was adjusted so that it occurs around the six o'clock position for the blade and avoids the milling zone.

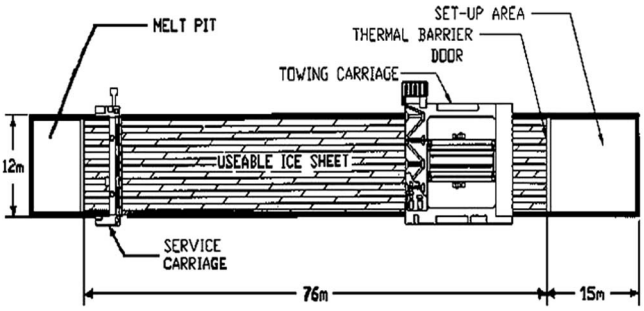

Fig. 5 Schematic diagram of the ice tank at the NRC-IOT

Results

Earlier dimensional analyses established that the expected significant variables during propeller-ice interaction are compressive strength of the ice, depth of cut, rps, and carriage speed [29]. In

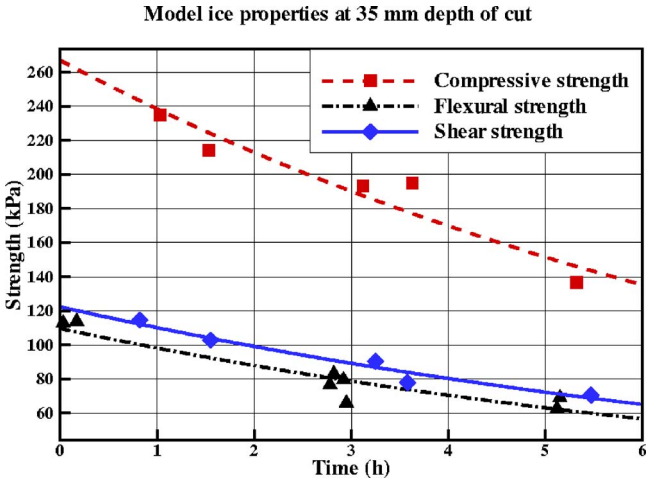

Fig. 6 Model ice properties versus time for 35 mm depth of cut case (tests were carried out between two and three hours marks of the time axis; mean value of the compressive strength for the present runs was approximately 210 kPa)

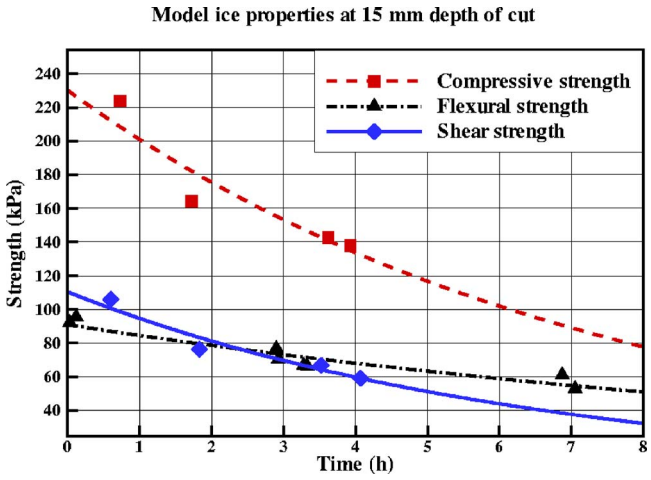

Fig. 7 Model ice properties versus time for 15 mm depth of cut case (tests were carried out at around five hours mark of the time-axis; mean value of the compressive strength for the present runs was approximately 120 kPa)

order to determine the contribution of each variable to the "*ice-related*" loads, data were analyzed to obtain the maximum, minimum and average values for the milling periods as shown as open triangles in Fig. 9. Thus, the basic statistics presented in the following sections are calculated for the milling periods only.

Table 1 Test matrix

Depth of cut (mm)	RPS	Carriage speed (m/s)	No. of tests
35	5, 7, 10	0.2, 0.5, 0.8	One time at each condition
15	5, 7	0.2, 0.5, 0.8	Three times at each condition

Table 2 Milling angle versus depth of cut

Depth of cut (mm)	Estimated milling angle (α_m) (deg)
15	69
35	105

Figure 10 shows nondimensional average axial loads, i.e., average blade thrust coefficient ($K_{T(\text{Blade})}$) against advance coefficient for milling periods. The blade thrust coefficient is defined in Eq. (2) and the average F_X was obtained from the milling periods. For the advance coefficient ($J=V_A/(nD)$), the advance speed (V_A) was taken as the carriage speed (V).

$$K_{T(\text{Blade})} = \frac{F_{X(\text{Blade})}}{\rho n^2 D^4} = \Phi\left(\frac{V_A}{nD}\right) \tag{2}$$

The results of the 15 mm and the 35 mm depth of cut are compared with the results of the previous tests [15], which used a highly skewed propeller with different depths of cut: 20.5, 34, and 43 mm. The highly skewed propeller tests were carried out in the same EG/AD/S model ice as the present tests. However, the geometry of the highly skewed propeller was considerably different from the geometry of the propeller used in the present model. Data analysis methods employed in the two studies were also different, because the model used in the highly skewed propeller tests did not have the capability to measure the angular position of the blade(s). In [15], the milling period was estimated based on the variations in the measured loads. This may cause discrepancies in the magnitudes of the blade thrust coefficients ($K_{T(\text{Blade})}$) between the two tests.

The results in Fig. 10 illustrate that mean blade thrust coefficients increase with advance coefficients until a certain value of advance coefficient is reached (between 0.3 and 0.4 in Fig. 10), after which a decrease is observed. Based on the results of the tests with a highly skewed propeller, Fig. 10 also shows that as the depth of cut increases, so does the advance coefficient corresponding to the peak of the blade thrust coefficient curve. In the case of

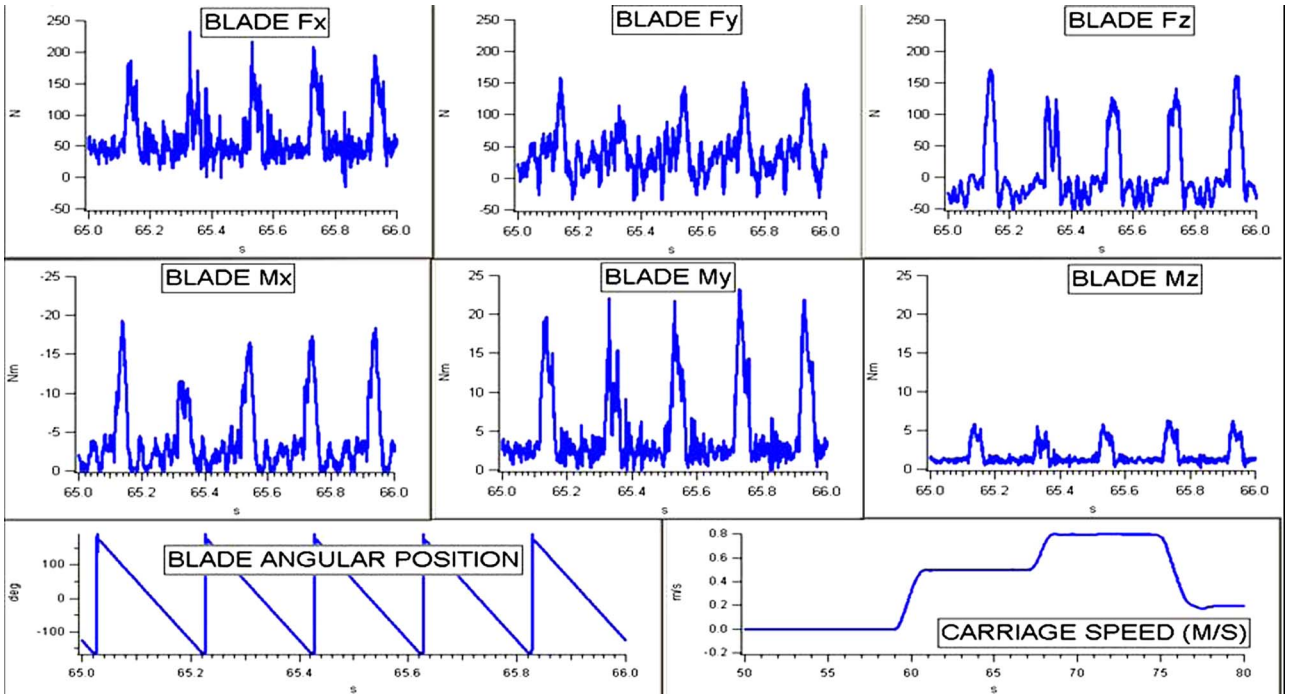

Fig. 8 Time series data from the experimental tests

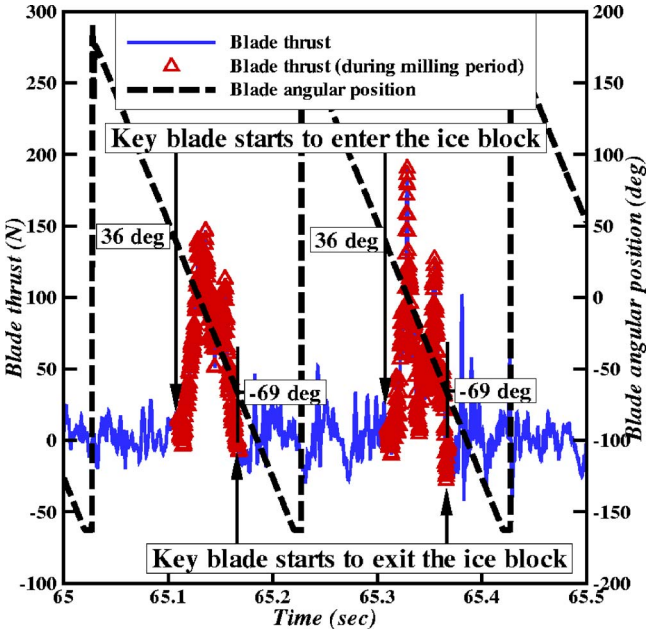

Fig. 9 Blade thrust during ice milling based on the milling angle (α_m: from 36 deg to –69 deg, 35 mm depth of cut at 5 rps)

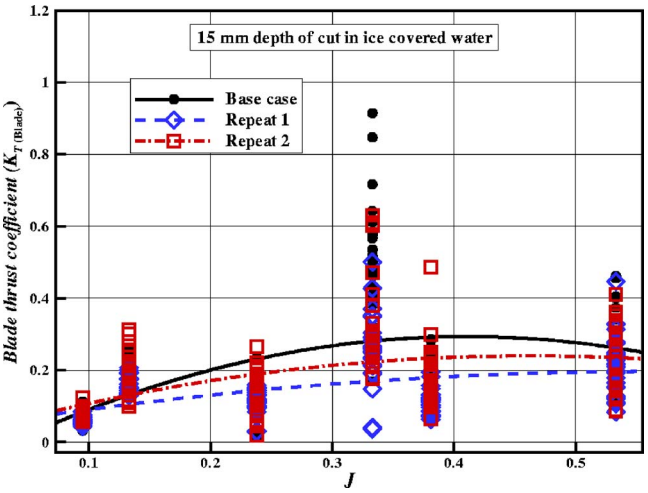

Fig. 11 Maximum blade thrust coefficients ($K_{T(Blade)}$, one blade only) for the 15 mm depth of cut in the repeat tests ("*ice-related*" loads during milling period)

the 35 mm depth of cut from the present experiments, however, the results do not seem to ever reach the peak value similar to the others for the advance coefficient range given in the figure. In general, a high depth of cut leads to a high thrust coefficient corresponding to the peak of the blade thrust coefficient curve.

Figure 11 shows the results of the repeat tests for the case of 15 mm depth of cut. The symbols represent the maximum values observed during milling periods for each test, and the lines through these points represent second order polynomial lines of the best fit. Each case in the figure, base case and the two repeats, consisted of three different carriage velocities (0.2, 0.5, and 0.8 m/s) conducted at two different rps values: 5 and 7. Since the time each case done and the section of the ice sheet used for each case were different, ice properties encountered during the tests were possibly different. This is because of the spatial and temporal variations of the model ice. The "Base case" and "Repeat 1" were tested consecutively in the Centre Channel of the same ice sheet, and "Repeat 2" was tested an hour later in the South Channel. The estimated compressive strengths for "Base case," "Repeat 1," and "Repeat 2" were 131.2, 129.0, and 107.4 kPa, respectively. The results show that the compressive strength of the ice over this range may not have significant effect on the magnitudes of the ice milling loads.

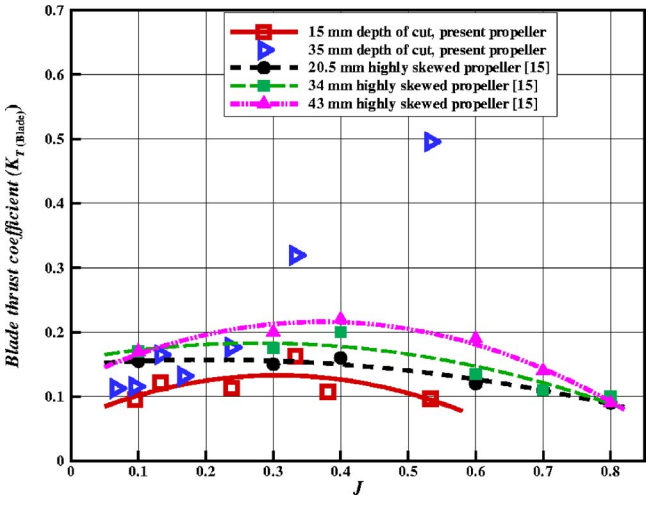

Fig. 10 Comparison of average blade thrust coefficient ($K_{T(Blade)}$, one blade only) with previous test results ("*ice-related*" loads+"*separable*" hydrodynamic loads during milling period). The lines are the second order polynomial lines of best fit [15].

The large scatter in $K_{T(Blade)}$, which appears at the advance coefficient of 0.33 in "Base case," may have been caused by the variations in the ice properties and the way interactions with the ice occurred. It was observed during the experiments that some pre-sawn ice blocks accelerated and moved towards the propeller, causing additional impact loads rather than pure milling loads only. Note that the ice sheet was pre-sawn to reduce the crushing loads on the strut of the model propulsor. Also, it was noticed that the key blade did not always contact the ice block because of the shadowing or the ice spalling, cracking, or damage from the previous blade(s). The variability range in the figure is approximately from $K_{T(Blade)}$=0.17 to 0.914 for "Base case."

Figure 12 shows the basic statistics for shaft thrust coefficient for the propeller-ice interaction periods of the tests with 35 mm depth of cut. Squares, triangles, and diamonds denote the maximum, average, and minimum of the shaft thrust coefficients, respectively. When the advance coefficients are less than 0.2, the average shaft thrust values measured during the interaction periods match well with those obtained in open water condition. In other words, at the lower advance coefficients ($J<0.2$), the interaction with ice did not significantly affect the average shaft thrust values of the propeller in Fig. 12. The maximum and minimum values, on the other hand, have a diverging trend with respect to the average values as advance coefficients increase. At the maximum, the maximum values were 350% higher than the average values and the minimum values were 180% lower than the average values. Though not reported in this paper, similar findings were observed for the test results with 15 mm depth of cut.

Similar results are given for shaft torque in Fig. 13 for the tests with 35 mm depth of cut. The solid line without symbols shows the average shaft torque from open water tests. Three different propeller speeds were used in these tests: 5, 7, and 10 rps. Solid squares with solid line, solid squares with dotted line, and open squares with solid line denote the shaft torque coefficients based on the maximum values measured during the ice milling periods for 5, 7, and 10 rps, respectively. These tests were carried out within an hour after the first test in this series in the same ice

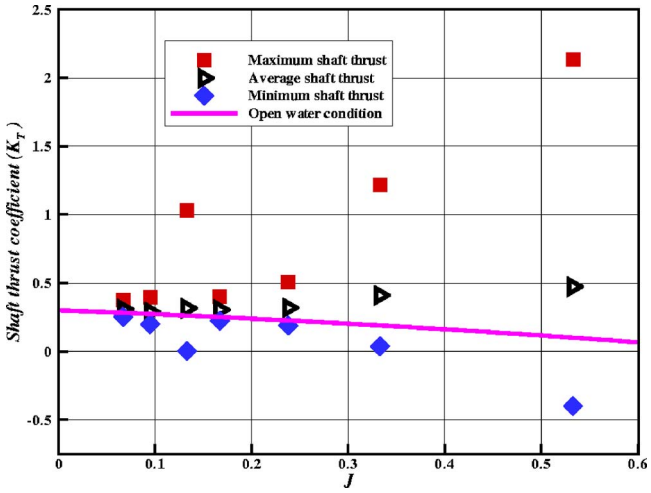

Fig. 12 Maximum, minimum, and average values for shaft thrust for 35 mm depth of cut ("*ice-related*" loads +"*separable*" hydrodynamic loads during milling period) and open water tests

channel. The range of measured compressive strength values for ice varied from 210 to 190 kPa. The average shaft torques in the ice milling period are higher than those in open water condition. As percentage, the increases in the average shaft torques from open water condition to ice milling condition are higher than the increases for the average thrust values.

Consequently, the propeller efficiency decreases in ice operation. The results also show that the case with lower rps requires a higher shaft torque. A possible explanation is given below.

Let's sketch a blade's position in ice as shown in Fig. 14. β_i is the angle of advance as defined in Eq. (3) for each rps value.

$$\beta_i = \arctan\left(\frac{V_A}{2\pi n_i r}\right) \tag{3}$$

where V_A is equal to V, n is rps, i is the index for rps (1, 2 and 3 are for 10, 7, and 5 rps), and r is the radius at the blade section considered. While the distance between two consecutive blades of the propeller are the same, the axial ice contact length, $V/(Zn_i)$, between the two consecutive blade passes varies because of the differences in the propeller rotational speeds for a given advance

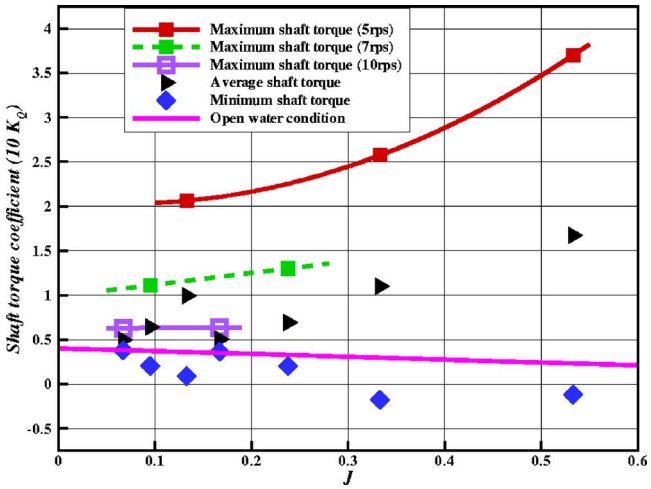

Fig. 13 Maximum, minimum, and average shaft torque for the 35 mm depth of cut ("*ice-related*" loads+"*separable*" hydrodynamic loads during milling period) and open water tests

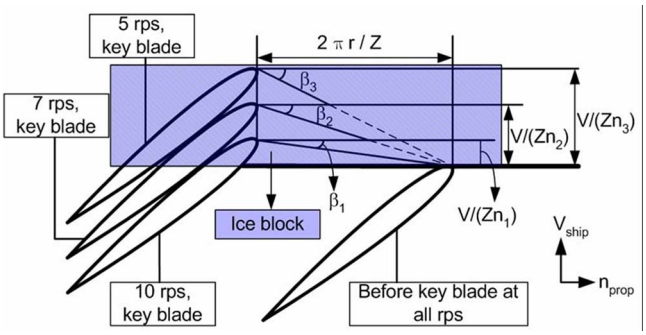

Fig. 14 Conceptual sketch for the propeller ice interaction with top view, where β is the angle of advance, r is the radius at the blade section considered, Z is number of blades (4), V is carriage speed, and n_1, n_2 and n_3 are 10, 7, and 5 rps, respectively

velocity. As shown in Fig. 14, the blade with the lower rps experiences the largest angle of advance, β, and thus the longest axial ice contact length among the three, and this may be the reason for the largest torque measured in the slowest rps case. For a given advance velocity (V), milling angle (α_m), and rotational speed (n), the amount of time, which a blade will be in contact with ice, is $(\alpha_m/2\pi)(1/n)$, and the distance traveled parallel to V during this time is $(\alpha_m/2\pi)(1/n)V$. It is evident from this that for a given V and α_m, the slower the rps is the longer this axial distance is. As this distance increases, the area of the blade in contact with ice increases and the likelihood of encountering the groove made by the preceding blade pass decreases, as depicted in Fig. 14. Therefore, it is expected that for a given advance velocity and depth of cut (or α_m), the cases with slower rps values may result in higher torque coefficients. In Fig. 13, the K_Q-J curves for each n value are fairly distinct from each other. This may suggest that the differences of the magnitudes of torque coefficients for a given advance coefficient are likely caused by the effects of rps. It is noted that the maximum shaft thrust coefficients, as shown in Fig. 12, have a similar trend as the maximum torque coefficients although the data points for different rps values are not marked clearly.

In an earlier study, Luznik [18,19] gives the results of his study for a very similar propeller geometry to the one used in the present study operating in the vicinity of an ice block-blockage condition. They reported an increase of 65–75% in the shaft thrust coefficient from the uniform flow performance. Figure 15 shows the comparison of the shaft thrust coefficients from open water, ice blockage, and ice milling conditions. The solid line shows the thrust coefficient in open water conditions, and the dashed line shows the maximum possible thrust coefficient in blocked flow. It is noted that the results from blockage condition are obtained from Luznik [18,19]. Solid triangles and solid circles show the maximum total loads in ice for the 15 and 35 mm depths of cut, respectively.

In Fig. 15, the highest three values of the shaft thrust coefficients corresponding to the advance coefficients of 0.133, 0.33, and 0.53 are for the 35 mm depth of cut tests performed at 5 rps. As explained in Figs. 12 and 13, for a constant carriage speed, the lower rps leads to a higher axial contact length, $V/(Zn_i)$. As long as the effective angle of attack is positive, the increase in the axial contact length helps to increase the thrust. However, in the case of 15 mm depth of cut, the nominal blade pitch angle for the region of the blade inside the ice is less than that of the case with 35 mm depth of cut. This may cause a decrease in the thrust coefficient at high advance coefficients due to small or negative angles of attack compared to those of the 35 mm depth of cut tests. Generally, maximum shaft thrusts in ice are higher than those in open water.

Figures 16 and 17 show the comparison with the existing ice load models from the JRPA #6 and International Association of

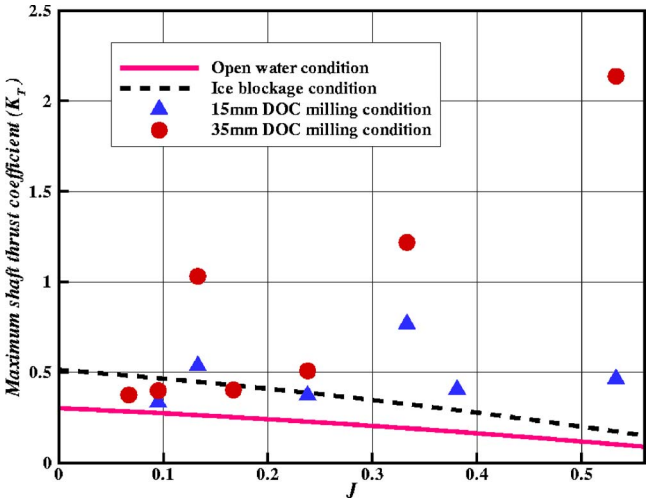

Fig. 15 Thrust coefficient comparison among open water, ice blockage, and ice milling conditions (for 15 and 35 mm depth of cut (DOC): "*ice-related*" loads+"*separable*" hydrodynamic loads during milling period)

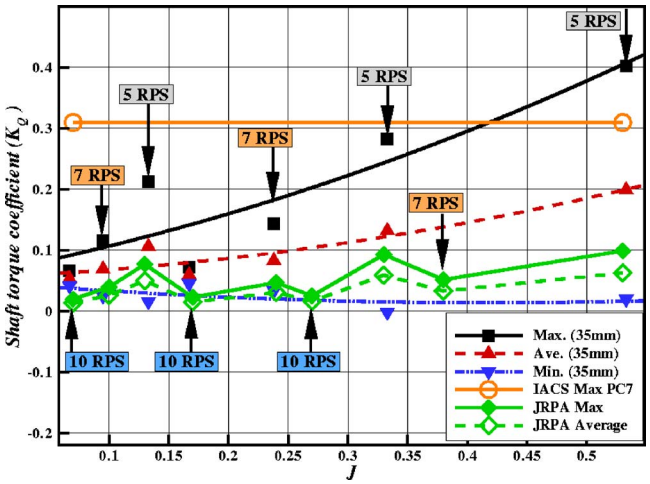

Fig. 17 K_Q comparison with ice load models (present test results: 35 mm depth of cut case, "*ice-related*" loads +"*separable*" hydrodynamic loads during milling period)

Classification Societies [30,31]. The IACS requirements are composed of seven different ice classes, PC1 to PC7, for which increasing number indicates that the ice properties including thickness and strength becomes thinner and weaker. For the comparison, the present model test results of the 35 mm depth of cut case were used. Nondimensional shaft thrust and torque coefficients are calculated during the milling period with "*ice-related*" loads and "*separable*" hydrodynamic loads. A scale factor of 13.733 is applied to dimensional variables for the ice load models.

Both JRPA #6 and IACS models consider the effect of rps; as the rps increases, the magnitudes of the thrust/torque coefficients decrease. As the ice class number in the IACS model decreases, the maximum thrust values remain constant (only minimum thrust values vary). For the IACS model in Figs. 16 and 17, the rps used in calculations was 1.35, which is equivalent to the 5 rps case in the model tests. The effects of angle of attack and advance coefficient are taken into account for the thrust and torque calculations in the JRPA #6 model, except in the maximum thrust value.

In Fig. 16, the gray area shows the range of the JRPA #6 model. For most values of advance coefficient, our measurements fall within the JRPA #6 range. At the advance coefficient of 0.53, both the maximum and minimum shaft thrust magnitudes from the JRPA #6 are slightly lower than those from the measurements, while the IACS model shows somewhat underestimated maximum and overestimated minimum shaft thrust values in terms of the magnitude.

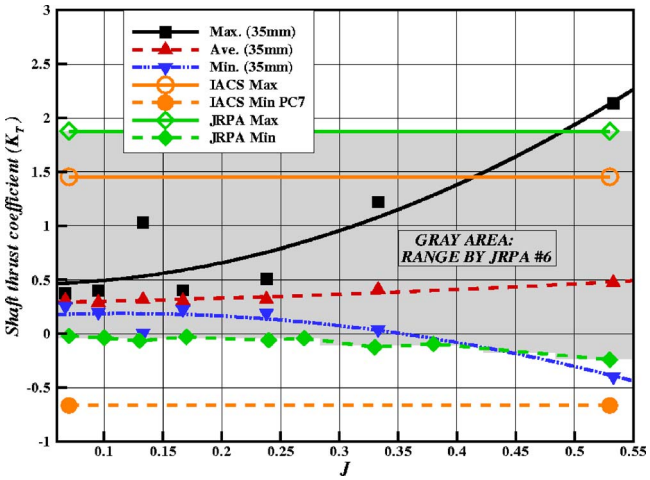

Fig. 16 K_T comparisons with ice load models (present test results: 35 mm depth of cut case, "*ice-related*" loads +"*separable*" hydrodynamic loads during milling period)

In Fig. 17, the maximum torque values from the IACS shown are slightly lower than those from the present measurements at the advance coefficient of 0.53, but the average or maximum torque values from the JRPA #6 are lower than the most average torque values from the present measurements. Although the JRPA #6 model gives underestimated torque coefficient values, the trends of lower rps causing higher torque values are the same as the findings of this study.

It is noted that the IACS model presented in this paper did not consider any shaft dynamic effects. The JRPA #6 model used the depth of cut of 35 mm multiplied by scale ratio as the JRPA #6 model required value in full scale for the ice block thickness.

Conclusion and Discussion

Experiments were conducted in an ice tank to determine the ice loads experienced by the blades of a podded propulsor operating in ice. The total loads in ice covered and open water were compared to each other and the difference between them denoted as "*ice-related*" loads.

Generally blade thrust coefficients for tests in ice covered water were found to increase with advance coefficient up to a certain value and then decrease as the advance coefficient increased further. Comparison of the present test results with the previous test results for a highly skewed propeller showed generally good agreement for the trends in the loads measured. However, the comparisons for the 35 mm depth of cut case were not as good as those for the 15 mm depth cut case.

From the repeat tests at 15 mm depth of cut, the effect of the compressive strength was investigated. The results, however, show that the compressive strength, within the range from 131.2 to 109 kPa, did not significantly affect the blade thrust or ice milling loads. At an advance coefficient of 0.33, significant variability was found in maximum thrust values, which might have been due to the irregularities in the ice properties and ice feeding into the propeller as well as the nature of the ice loading.

The maximum, average, and minimum shaft thrust coefficients at the 35 mm depth of cut were examined. The results showed a large variation in the ice milling loads with a maximum of 350%

increase in the magnitude of the maximum, and a maximum of 180% decrease in the magnitude of the minimum shaft thrust from the average values.

The effect of the shaft speed on the maximum torque was investigated. The lower rps required a relatively higher shaft torque because of the increases in the angle of advance and the axial contact length (ice contact area) at the given test conditions.

Comparison of ice milling results for the 15 and 35 mm depths of cut with hydrodynamic loads including the blockage condition was done. Noncontact hydrodynamic loads in the blockage condition are at the maximum 65–75% higher than those in open water test conditions [18,19]. Generally, higher depths of cut produce more thrust in ice covered water tests and the thrust readings in ice covered water tests are always higher than those from open water conditions. The results show that the total "*ice-related*" loads are strongly dependent on the depth of cut and advance coefficient.

Two ice load models from the JRPA #6 and IACS are presented and compared with the present test results. The maximum and minimum shaft thrust coefficients from the JRPA #6 model show a good agreement with those from the present measurements. The maximum and average shaft torque values from the JRPA #6 are smaller than the most average shaft torque values from the present measurements, but the trends in the results are well matched qualitatively in torque comparison; the decrease in rps resulted in an increase in the magnitude of the torque coefficient. The shaft thrust and torque coefficients from the IACS model are mostly well predicted until the advance coefficients reach 0.4. When the advance coefficient goes over 0.4, the maximum shaft thrust and torque coefficients are smaller than those from the present measurements.

The analysis shows variability of measured data. The variability of data is associated with several factors:

- Pre-sawn ice blocks were observed to be accelerating towards the propeller blades due to the suction from the propeller. Though this phenomenon was regularly occurring, it is thought to be a contributory factor in the variability.
- Ice properties vary depending on location across the ice sheet.
- The irregularity in the ice thickness along the path of the propeller may lead to a change in the depth of cut.

For the "*ice-related*" loads, the shaft thrust values were obtained from the milling period. This may miss the real maximum because there were four blades, but only one was instrumented. However, the number of blade impacts with ice is several hundred and so it is expected that the mean values would be approximately the same.

Acknowledgment

This study on podded propellers is a joint project between Transport Canada and the National Research Council of Canada and we thank Victor Santos-Pedro, Director, Design, Equipment and Boating Safety, Marine Safety, Transport Canada for continued support of our research.

We would also like to acknowledge the financial and in-kind support for the research provided by the Korea Research Foundation Grant (KRF-2004-042-D00236), the Advanced Ship Engineering Research Center in Pusan National University, and the National Science and Engineering Research Council of Canada.

Furthermore, thanks are due to Memorial University's Technical Services Department for their help in the experimental work. Special thanks are extended to the members of the National Research Council of Canada's Institute for Ocean Technology for their assistance in various stages of this project.

Nomenclature

D = propeller diameter (m)
F_X = force in direction of x axis
F_Y = force in direction of y axis
F_Z = force in direction of z axis
F_B = total blade foce $(F_X^2+F_Y^2+F_Z^2)^{1/2}$
J = advance coefficient $(V_A/(nD))$
K_T = shaft thrust coefficient
K_Q = shaft torque coefficient
$K_{T(\mathrm{Blade})}$ = blade thrust coefficient
M_X = moment about x axis
M_Y = moment about y axis
M_Z = moment about z axis
r = radius at the blade section considered (m)
n = propeller rotating speed (Revolution Per Second)
V_A = advance speed (m/s)
V = carriage speed (m/s)
Z = number of Blades
α_m = milling angle (degrees)
β = angle of advance (degrees)
ρ = density of water (kg/m^3)

References

[1] Laskow, V., and Revill, C., 1986, "Engineering Analysis of Ice/Propeller Interaction Data," Transportation Development Centre Report, TP 8450E.
[2] Jussila, M., and Koskinen, P., 1989, "Ice Loads on CP-Propeller and Propeller Shaft of Small Ferry and Their Statistical Distributions During Winter '87," *Proc. 8th International Conference on Offshore Mechanics and Arctic Engineering (OMAE'89)*, Netherlands, March 19-23, Vol. 4, pp. 351–358.
[3] Keinonen, A., Browne, R., and Jacobsen, C., 1990, "Ice Propeller Interaction Forces," Transportation Development Centre Report, TP 10401E.
[4] Williams, F., Spencer, D., Mathews, S., and Bayly, I., 1992, "Full Scale trials in Level Ice With Canadian R-Class Icebreaker," Soc. Nav. Archit. Mar. Eng., Trans., **100**, pp. 293–313.
[5] Cowper, B., Browne, R., Glen, I., and Ritch, R., 1992, "Resistance and Propulsive Performance Trials of the MV Terry Fox and MV Ikaluk in Level Ice," Soc. Nav. Archit. Mar. Eng., Trans., **100**, pp. 315–343.
[6] Jussila, M., and Soininen, H., 1991, "Interaction Between Ice and Propeller," Research Reports 1281, Technical Research Centre of Finland, Espoo.
[7] Newbury, S., Shih, L., Browne, R., Revill, C., Kenny, S., and Zheng, Y., 1993, "Experimental and Theoretical Evaluation of Hydrodynamic Pressure During Non-contact Propeller/Ice Interaction," *Proc. 2nd Canadian Marine Dynamics Conference*, Vancouver, August 9-11, pp. 157–166.
[8] Newbury, S., Browne, R., and Jones, S., 1994, "Experimental Determination of Hydrodynamic Non-contact Loads During Propeller-Ice Interaction," *Proc. 4th International Society of Offshore and Polar Engineers (ISOPE'94)*, Osaka, April 10-15, Vol. 2, pp. 596–601.
[9] Browne, R., 1997, "Analysis of Canadian Full Scale Propeller and Ice Interaction Trials Data for Correlation With Empirical Models," Report No. CR-1997-12, Institute for Ocean Technology, National Research Council of Canada.
[10] Jones, S. J., Soininen, H., Jussila, M., Koskinen, P., Newbury, S., and Browne, R., 1997, "Propeller-Ice Interaction," Soc. Nav. Archit. Mar. Eng., Trans., **105**, pp. 399–425.
[11] Veitch, B., 1995, "Predictions of Ice Contact Forces on a Marine Screw Propeller During the Propeller-Ice Cutting Process," Acta Polytechnica Scandinavica, Mechanical Engineering Series, Helsinki, p. 118.
[12] Soininen, H., 1998, "A Propeller-Ice Contact Model," Dissertation for the Degree of Doctor of Technology, Helsinki University of Technology, Espoo.
[13] Searle, S., Veitch, B., and Bose, N., 1999, "Ice-Class Propeller Performance in Extreme Conditions," Soc. Nav. Archit. Mar. Eng., Trans., **107**, pp. 127–152.
[14] Moores, C., Veitch, B., Bose, N., Jones, S. J., and Carlton, J., 2002, "Multi-Component Blade Load Measurements on a Propeller in Ice," Soc. Nav. Archit. Mar. Eng., Trans., **110**, pp. 169–188.
[15] Moores, C., 2002, "Shaft and Blade Load Measurements on a Highly Skewed Propeller Model in Ice," Master of Engineering Thesis, Memorial University of Newfoundland, St. John's, Newfoundland.
[16] Doucet, J., Liu, P., and Bose, N., 1998, "Numerical Prediction of Ice-Induced Loads on Ice-Class Screw Propellers Using a Synthesized Contact/Hydrodynamic Code," Ocean Engineering Research Centre Report No. OERC-1998–004.
[17] Walker, D., Bose, N., and Yamaguchi, H., 1994, "Hydrodynamic Performance and Cavitation of an Open Propeller in a Simulated Ice Blocked Flow," ASME J. Offshore Mech. Arct. Eng., **116**, pp. 185–189.
[18] Luznik, L., 1994, "Open Water Performance of a Propeller in a Uniform Flow and in a Blocked Flow from a Nearby Simulated Ice Body," Memorial University of Newfoundland, OERC Report No. WR-WTT-94001.
[19] Luznik, L., Walker, D., Bose, N., and Jones, S. J., 1995, "Effects of Ice Blockage Size and Proximity on Propeller Performance During Non-Contact Propeller Ice Interaction," *Proc. 14th International Conference on Offshore Mechan-*

ics and Arctic Engineering, (OMAE'95), Copenhagen, June 18-22, Vol. 4, pp. 35–39.
[20] Bose, N., 1996, "Ice Blocked Propeller Performance Prediction Using a Panel Method," Trans. RINA, **138**, pp. 213–226.
[21] Liu, P., Doucet, M., Veitch, B., Robbins, I., and Bose, N., 2000, "Numerical Prediction of Ice Induced Hydrodynamic Loads on Propellers due to Blockage," J. Ocean. Eng. Int., **4**(1), pp. 31–38.
[22] Akinturk, A., Jones, S., Duffy, D., and Rowell, B., 2004, "Ice Loads on Azimuthing Podded Propulsors," *Proc. 23rd International Conference on Offshore Mechanics and Arctic Engineering, (OMAE'04)*, New York, June 20-25 (CD-ROM, no page numbers).
[23] Wang, J., Akinturk, A., Foster, W., Jones, S. J., and Bose, N., 2004, "An Experimental Model for Ice Performance of Podded Propellers," *Proc. of the 27th American Towing Tank Conference*, Institute for Ocean Technology, National Research Council of Canada, August 6-7 (CD-ROM, no page numbers).
[24] Wang, J., Akinturk, A., Jones, S. J., and Bose, N., 2005, "Ice Loads on a Model Podded Propeller Blade in Milling Conditions," *Proc. 24th International Conference on Offshore Mechanics and Arctic Engineering, (OMAE'05)*, Halkidiki, Greece, June 12-17 (CD-ROM, no page numbers).
[25] Emerson, A., and Sinclair, L., 1978, "Propeller Design and Model Experiments," Trans. North East Coast Institution of Engineers and Shipbuilders, **94**, pp. 199–234; 1978, "Propeller Design and Model Experiments," Trans. North East Coast Institution of Engineers and Shipbuilders **94**, D31–34.
[26] Jones, S. J., 1987, "Ice Tank Test Procedure at the Institute for Marine Dynamics," Report No. LM-AVR-20, Institute for Ocean Technology, National Research Council of Canada.
[27] Timco, G., 1986, "EG/AD/S: A New Type of Model Ice for Refrigerated Towing Tanks," J. Cold Sci. Technol., **12**, pp. 175–195.
[28] Spencer, D. S., and Timco, G. W., 1990, "CD Model Ice: a Process to Produce Correct Density (CD) Model Ice," *Proc. 10th IAHR Symposium on Ice*, Espoo, Finland, August 20-24, Vol. 2, pp. 745–755.
[29] Sharp, J. J., Deb, A., and Deb, M. K., 1992, "Application of Matrix Manipulation in Dimensional Analysis Involving Large Numbers of Variables," Mar. Struct., **5**(4), pp. 333–348.
[30] Koskinen, P., Jussila, M., and Soininen, H., 1996, "Propeller Ice Load Models," Research Reports 1739, Technical Research Centre of Finland, Espoo.
[31] International Association of Classification Societies (IACS), 2006, I3 Machinery Requirement for Polar Class Ships.